CDF note 7835

Search for Pair Production of Scalar Top Quarks Decaying to a τ Lepton and a b Quark

The CDF Collaboration
URL http://www-cdf.fnal.gov
(Dated: September 15, 2005)

We present the results of a search for pair production of scalar top quarks ($\tilde{t}_1$) in an R-parity violating supersymmetry scenario in 322 pb^{-1} of $p\overline{p}$ collisions at $\sqrt{s}$ = 1.96 TeV collected by the Collider Detector at Fermilab. In this case each $\tilde{t}_1$ decays into a τ lepton and a b quark. The final state is either an electron or a muon ($\ell = e$ or μ) from the $\tau \to \ell \nu_\ell \nu_\tau$ decay, as well as a hadronically decaying τ lepton, and two or more jets. Two candidate events pass our final selection criteria, which is consistent with the standard model expectation of $2.26^{+0.46}_{-0.22}$ events. We set a 95% confidence level lower limit on the $\tilde{t}_1$ mass, $m(\tilde{t}_1)$, at 155 GeV$/c^2$ for $\mathscr{B}(\tilde{t}_1 \to \tau b) = 1$ with the next-to-leading order calculation of the cross section. If we include theoretical uncertainties in the cross section calculation due to the renormalization scales and PDFs, a conservative limit of $m(\tilde{t}_1) > 151$ GeV$/c^2$ is obtained. These limits are also fully applicable to the case of the third generation scalar leptoquark (LQ_3) assuming a 100% branching ratio for the $LQ_3 \to \tau b$ decay mode.

I. INTRODUCTION

Various supersymmetric (SUSY) models [1] predict that the first two generations of SUSY partners of the quarks and the leptons (squarks and sleptons) are approximately mass degenerate. However, the mass of the lightest scalar top quark ($\tilde{t}_1$ or 'stop') can be relatively light due to a large mixing between the interaction eigenstates, $\tilde{t}_L$ and $\tilde{t}_R$. This mixing depends in part on the top Yukawa coupling which is largely due to the heavy top quark mass, and it is possible that $\tilde{t}_1$ is lighter than the top quark [2]. Within a framework of R_p violating ($\not{R}_p$) SUSY [3], each $\tilde{t}_1$ decays to a tau (τ) lepton and a bottom (b) quark with a branching ratio, $\mathscr{B}$, which depends on the coupling constants of the particular model.

In $p\overline{p}$ collisions at $\sqrt{s} = 1.96$ TeV at the Fermilab Tevatron, stop pairs might be produced strongly via R_p-conserving processes through gg fusion and $q\overline{q}$ annihilation. In this paper we describe a search for $\tilde{t}_1\bar{\tilde{t}}_1 \to \tau\tau b\overline{b}$ with the CDF II detector [4] in a final state of either an electron or a muon ($\ell = e$ or μ) from the $\tau \to \ell\nu_\ell\nu_\tau$ (τ_ℓ) decay, a hadronically decaying tau (τ_h) lepton, and two or more jets. We assume $\mathscr{B}(\tilde{t}_1 \to \tau b) = 1$.

II. DATA SAMPLE AND EVENT SELECTION

The analysis begins with a data sample collected by inclusive lepton plus track triggers [5] that require an electron candidate with calorimeter cluster $E_\mathrm{T} > 8$ GeV ($|\eta| < 1.1$ [6] in CEM [7]) or a muon candidate with track momentum $p_\mathrm{T} > 8$ GeV$/c$ ($|\eta| < 0.6$ in CMUP; $0.6 < |\eta| < 1$ in CMX), and an additional XFT track with $p_\mathrm{T} > 5$ GeV$/c$. The integrated luminosity of the data sample for CEM and CMUP (CMX) is 322 pb^{-1} (304 pb^{-1}).

We select events by identifying at least one lepton with ${p_\mathrm{T}}^\ell > 10$ GeV$/c$ for the CEM electron, CMUP or CMX muon) and at least one τ_h candidate with ${p_\mathrm{T}}^\tau > 15$ GeV$/c$ in the fiducial region of the detector. Jets are identified with a fixed-cone of $\Delta R = 0.4$ in $|\eta| < 2.4$ and required to have $E_\mathrm{T} > 20$ GeV and separated from any of e, μ, and τ_h by $\Delta R > 0.8$.

We then apply for a series of event topology cuts designed to improve the sensitivity of the search, where the dominant standard model (SM) backgrounds are QCD events ($b\overline{b}$, $\gamma +$ jet) and vector bosons with multiple jets. The events are removed if (a) the primary electron is from photon conversion or the primary muon is a cosmic ray muon; (b) the invariant mass of the primary electron and a loosely-identified second electron candidate is $76 < m_{e^+e^-} < 106$ GeV$/c^2$; (c) the invariant mass of the primary electron and its hadronic tau partner is $76 < m_{e\tau} < 106$ GeV$/c^2$ and they are separated with $\Delta\phi_{e\tau} > 2.9$; (d) the invariant mass of the primary muon and a loosely-identified second muon candidate is $76 < m_{\mu^+\mu^-} < 106$ GeV$/c^2$; or (e) $S_\mathrm{T} \equiv {p_\mathrm{T}}^\ell + {p_\mathrm{T}}^{\tau_\mathrm{h}} + \not{E}_\mathrm{T} < 110$ GeV$/c$. Cut (e) is to suppress the QCD and $Z^0 \to \tau^+\tau^-$ events [8]. Cut (c) is to reject $Z^0 \to \tau^+\tau^-$ events where either e^- or e^+ is misidentified as a τ_h. For the muon channel we do not use a cut similar to (c), as a probability for a muon to be reconstructed as τ_h is much smaller.

We define the primary signal region (A$_2$) with (f) $N_\mathrm{jet} \geq 2$ and (g) $m_\mathrm{T}(\ell, \not{E}_\mathrm{T}) < 35$ GeV$/c^2$ along with other five regions as defined in Table I. We determine the geometrical/kinematical acceptances ($A_\mathrm{geom/kine}$), efficiencies for identification (ID) and isolation (ISO) cuts (ε_ID and ε_ISO), lepton and XFT track trigger efficiencies ($\varepsilon^\ell_\mathrm{trig}$ and $\varepsilon^\mathrm{XFT}_\mathrm{trig}$), and the total acceptance for event topological cuts ($\varepsilon_\mathrm{topo}$), using PYTHIA [9] with the GEANT-based [10] CDF detector simulation or data. Our nominal choice of parton distribution functions (PDFs) and a renomalization scale (Q^2) is CTEQ6 [11] and $Q^2 = \sqrt{m(\tilde{t}_1)^2 + {p_\mathrm{T}}^2}$. These quantities numbers are summarized in Table II for $\tilde{t}_1\bar{\tilde{t}}_1(\to \tau_\ell\tau_\mathrm{h} b\overline{b})$ events ($m(\tilde{t}_1)$= 150 GeV$/c^2$) in region A$_2$. Figure 1 is the total event acceptance ($\alpha \equiv A_\mathrm{geom/kine} \cdot \varepsilon_\mathrm{ID} \cdot \varepsilon_\mathrm{ISO} \cdot \varepsilon_\mathrm{trig} \cdot \varepsilon_\mathrm{topo}$) as a function of $m(\tilde{t}_1)$. Here $\varepsilon_\mathrm{ID} = \varepsilon^\ell_\mathrm{ID} \cdot \varepsilon^{\tau_\mathrm{h}}_\mathrm{ID}$, $\varepsilon_\mathrm{ISO} = \varepsilon^\ell_\mathrm{ISO} \cdot \varepsilon^{\tau_\mathrm{h}}_\mathrm{ISO}$, $\varepsilon_\mathrm{trig} = \varepsilon^\ell_\mathrm{trig} \cdot \varepsilon^\mathrm{XFT}_\mathrm{trig}$.

It should be noted that to avoid biassing our result, a 'blind' analysis technique is employed, where the data in region A$_2$ is 'blinded' until we fully optimize the event selection criteria for signal events and estimate the signal event acceptance and the background (BG) events in each of six regions. At that point we freeze the criteria and examine the data in region A_2 for possible signal.

TABLE I: Definition of six regions in the m_T-N_jet plane, where A$_2$ is the primary signal region. Regions A$_0$, B$_0$, A$_2$ and B$_2$ are used in setting final limit, regions A$_1$ and B$_1$ will be used as control regions.

	$m_\mathrm{T} < 35$ GeV$/c^2$	$m_\mathrm{T} > 35$ GeV$/c^2$
$N_\mathrm{jet} \geq 2$	A$_2$	B$_2$
$N_\mathrm{jet} = 1$	A$_1$	B$_1$
$N_\mathrm{jet} = 0$	A$_0$	B$_0$

TABLE II: Acceptances and efficiencies (in %) for $\tilde{t}_1\bar{\tilde{t}}_1 \to \tau_\ell \tau_h b\bar{b}$ in region A_2 for the case of $m(\tilde{t}_1)$ = 150 GeV$/c^2$. Two systematic uncertainties are shown for $A_{\rm geom/kine}$, $\varepsilon_{\rm ID}$, $\varepsilon_{\rm ISO}$, and $\varepsilon_{\rm trig}$. The first is due to the statistical uncertainty since it is determined by MC or control data samples; second is the systematic uncertainty from the detector simulation.

	$e+\tau$	$\mu^{\rm CMUP}+\tau$	$\mu^{\rm CMX}+\tau$
$A_{\rm geom/kine}$			
Geometrical/kinematical acceptance for ℓ and τ_h with ΔR cut	$17.6 \pm 0.1 \pm 0.3$	$10.41 \pm 0.11 \pm 0.09$	$3.56 \pm 0.07 \pm 0.01$
$\varepsilon_{\rm ID}$			
Lepton identification efficiency	$83.8 \pm 0.4 \pm 0.9$	$84.9 \pm 0.3 \pm 3.7$	$91.0 \pm 0.6 \pm 0.3$
Tau identification efficiency	$75.2 \pm 0.5 \pm 2.2$	$74.0 \pm 0.6 \pm 2.2$	$71.8 \pm 1.1 \pm 2.2$
$\varepsilon_{\rm ISO}$			
Lepton isolation efficiency	$78.4 \pm 0.4 \pm 2.4$	$81.4 \pm 0.5 \pm 2.4$	$83.2 \pm 0.8 \pm 2.5$
Tau isolation efficiency	$70.0 \pm 0.6 \pm 2.1$	$70.9 \pm 0.7 \pm 2.1$	$70.4 \pm 1.3 \pm 2.1$
$\varepsilon_{\rm trig}$			
Lepton trigger efficiency	$97.6 \pm 0.2 \pm 1.0$	$95.8 \pm 0.3 \pm 1.0$	$94.6 \pm 0.5 \pm 1.0$
XFT-track trigger efficiency	$\longleftarrow$ $96.4 \pm 0.3 \pm 1.0$ $\longrightarrow$		
$\varepsilon_{\rm topo}$			
Total acceptance for event topology	40.7 ± 0.8	47.7 ± 1.0	47.1 ± 1.7
α : Total Event Acceptance	2.33 ± 0.06	1.65 ± 0.05	0.59 ± 0.03

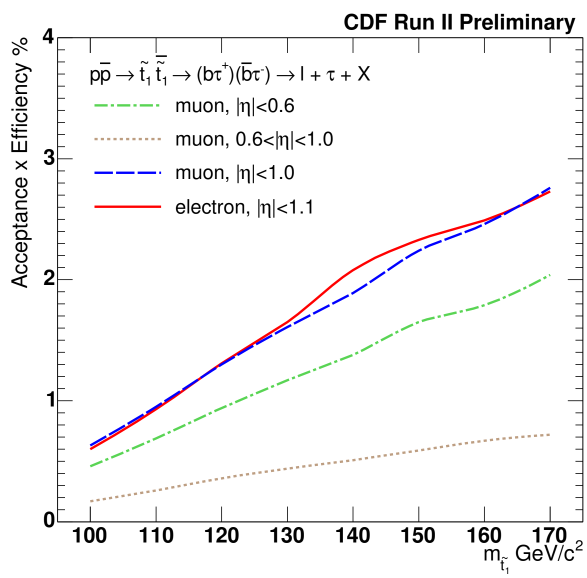

FIG. 1: Total event acceptance as a function of the stop mass, $m(\tilde{t}_1)$, for different lepton plus track triggers [5].

III. BACKGROUNDS

The SM backgrounds are (i) events with true $\ell\tau_h$ pair from $Z^0/\gamma^*(\to\tau^+\tau^-)$+jets, $t\bar{t}$ and diboson (W^+W^-, $W^\pm Z^0$, Z^0Z^0) production; (ii) events with fake $\ell\tau_h$ combination from $W+$jet, $Z^0/\gamma^*(\to\ell^+\ell^-)$+jets, and QCD events. We first estimate all SM background events excluding $W+$jet events. $Z^0/\gamma^*(\to\tau^+\tau^-)$+jets are estimated using PYTHIA [9] and the GEANT-based [10] CDF detector simulation with the correction factors for the $N_{\rm jet}$ distribution obtained from $Z^0\to\ell^+\ell^-$ data. The QCD events are estimated using the lepton ISO distribution using a data sample of non-isolated leptons. The contribution from $Z^0/\gamma^*(\to\ell^+\ell^-)$+jets, $t\bar{t}$ and W^+W^- production is estimated using with PYTHIA [9] and the detector simulation program. The contribution from $W^\pm Z^0$ and Z^0Z^0 is found to be negligible. The cross sections for $t\bar{t}$ and W^+W^- production are normalized to next-to-leading order (NLO) calculations of 6.7 and 12.4 pb, respectively.

In Table III we show the number of events observed in data, along with the expected number of SM events excluding the $W+$jet events. It should be noted that the number of events in data in region A_2 (shown in the boldface numbers) are only known after all event selection cuts are finalized and the SM backgrounds are estimated. The S_T distribution for a data sample of

TABLE III: Number of events observed in data, along with the expected number of SM background (BG) events excluding the $W+$jet contribution. The data in region A_2 is 'blinded' until we fully optimize the event selection criteria for signal events and estimate the signal event acceptance and the number of BG events in each of six regions.

	$e+\tau$ Channel		$\mu+\tau$ Channel	
Region	Observed	BG (excluding $W+$jet)	Observed	BG (excluding $W+$jet)
A_2	**1**	$1.27^{+0.29}_{-0.18}$	**1**	$0.99^{+0.35}_{-0.13}$
B_2	4	$2.62^{+0.42}_{-0.26}$	4	$2.19^{+0.39}_{-0.21}$
A_1	4	$3.07^{+0.39}_{-0.31}$	3	$2.74^{+0.57}_{-0.37}$
B_1	9	$2.45^{+0.36}_{-0.27}$	6	$2.36^{+0.50}_{-0.31}$
A_0	11	$7.92^{+0.69}_{-0.61}$	8	$5.05^{+0.64}_{-0.45}$
B_0	25	$5.34^{+0.63}_{-0.51}$	28	$5.80^{+0.74}_{-0.55}$

events with no extra jets, $S_T > 80$ GeV$/c$ and $m_T < 35$ GeV$/c^2$ is shown in Fig. 2, where the $W+$jet contribution is negligible. There is a good agreement between the data and the SM prediction. Our optimized cut on S_T is 110 GeV$/c$. We also show the $N_{\rm jet}$ distribution for events with $S_T > 110$ GeV$/c$ and $m_T < 35$ GeV$/c^2$ (regions A_0, A_1, and A_2) in Fig. 3.

A total of two events found in region A_2 are consistent with the SM expectation of $2.26^{+0.46}_{-0.22}$ events. We note that large discrepancies between 'Observed' and 'BG' in regions B_0 and B_1 are expected from the $W+$jet contribution. We estimate the $W+$jet contributions in A_2 and B_2 as $N^{W+j}(A_2) = N^{W+j}(A_0)\cdot\mathscr{R}_A$ and $N^{W+j}(B_2) = N^{W+j}(B_0)\cdot\mathscr{R}_B$, where $\mathscr{R}_A \sim \mathscr{R}_B$. The values of $\mathscr{R}$ for $m_T < 35$ GeV$/c^2$ and $m_T > 35$ GeV$/c^2$ are estimated with PYTHIA plus the detector simulation. We find the ratio of two $\mathscr{R}$ values to be 1.0 ± 0.5. The large uncertainty does not affect in setting the mass limit, because the $W+$jet contributions in regions A_2 and B_2 are negligible.

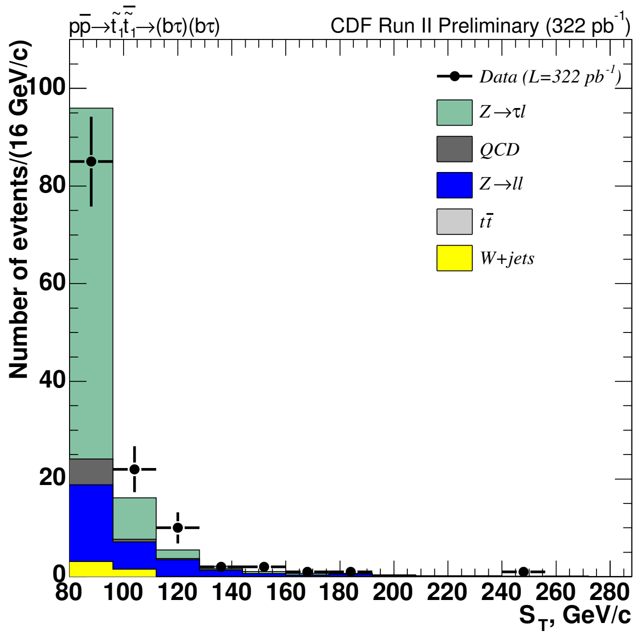

FIG. 2: Distribution of S_T in the data sample for events with no extra jets, $S_T > 80$ GeV$/c$ and $m_T < 35$ GeV$/c^2$ compared to the expectations from SM background events. The $\tilde{t}_1\bar{\tilde{t}}_1$ contribution for this region is negligible. For the final event selection we cut at $S_T > 110$ GeV$/c$.

IV. SYSTEMATIC UNCERTAINTIES

The sources of systematic uncertainties for the acceptance for $\tilde{t}_1\bar{\tilde{t}}_1 \to \tau_\ell\tau_h b\bar{b}$ are uncertainties from (a) PDFs, (b) initial and final state radiation (ISR and FSR), (c) jet energy scale, (d) $\not{E}_T$ simulation, (e) identification and isolation efficiencies for e,

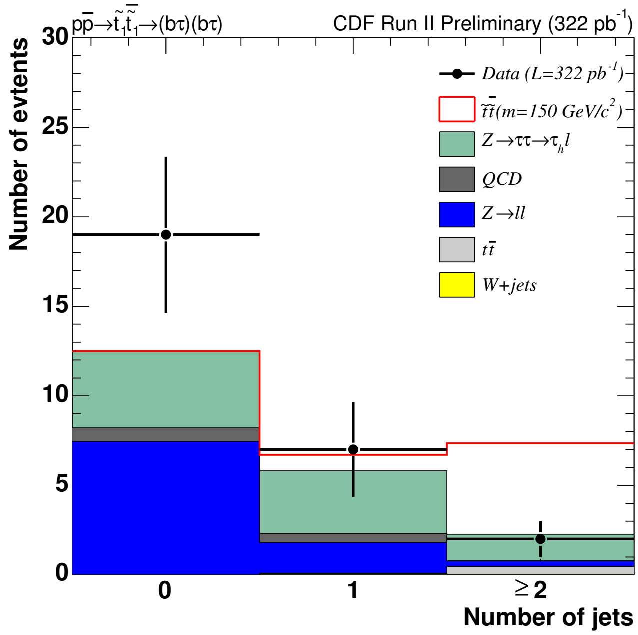

FIG. 3: Distribution of $N_{\rm jet}$ in the data sample in regions A_0, A_1, and A_2, compared to the expectations from SM background and $\tilde{t}_1\bar{\tilde{t}}_1$ ($m(\tilde{t}_1) = 150$ GeV$/c^2$) events.

μ, and $\tau_{\rm h}$, (f) geometrical and kinematical acceptance in the detector simulation. The combined systematic uncertainty for the electron (muon) channel varies from 10.7% (10.8%) for the stop mass of $m(\tilde{t}_1)$= 100 GeV$/c^2$ and 7.0% (7.2%) for 170 GeV$/c^2$.

V. CROSS SECTION AND MASS LIMITS

With no excess in region A_2, a 95% confidence level (C.L.) limit on the $\tilde{t}_1\bar{\tilde{t}}_1$ production cross section (σ) is calculated. We define a likelihood function using Poisson statistics as a function of σ using:

- Number of observed events in each of the regions A_2, B_2, A_0, and B_0;
- Number of expected events in each region, $N_i = \sigma\cdot\mathscr{B}(\tau\tau\to\tau_\ell\tau_{\rm h})\cdot\int\mathscr{L}\,dt\cdot\alpha_i + N_i^{\rm BG} + N_i^{W+j}$, where $N_i^{\rm BG}$ includes all SM backgrounds excluding $W+$jet events, α_i is the total event acceptance for signal in region i (note that α_i is negligibly small for regions A_0 and B_0);
- $\mathscr{R}_{\rm B}/\mathscr{R}_{\rm A} = 1.0\pm 0.5$, taking the absolute rate of the $W+$jet events as a nuisance parameter.

The likelihood function is a probability of observing the number of events found in data given the signal cross section. Electron and muon channels are treated as two separate measurements, taking into account correlated systematic uncertainties. It should be noted that the method has an advantage of including the expected signal events in region B_2 into setting the limits, which effectively increases the total signal event acceptance by approximately 40%.

Table IV shows 95% C.L. upper limits on the cross section as a function of $m(\tilde{t}_1)$. The 95% C.L. limit curve (thick solid line in red) is shown in Fig. 4, comparing to the NLO cross sections [12] for our nominal choice of CTEQ6M PDFs [11] and a renormalization scale of $Q^2 = \sqrt{m(\tilde{t}_1)^2 + p_T^2}$ (blue, solid), while two dashed lines with ± 18% uncertainties due to the choice of Q^2 (varying the scale from its nominal value by a factor of two or a half) and PDFs. We find $m(\tilde{t}_1) > 155$ GeV$/c^2$ for the nominal choice and a conservative mass limit of $m(\tilde{t}_1) > 151$ GeV$/c^2$. The previously published limit of $m(\tilde{t}_1) > 122$ GeV$/c^2$ [8] should be compared to 155 GeV$/c^2$.

It should be noted that the stop pair production process is very similar to the pair production of the third generation scalar leptoquark (LQ_3). The NLO cross section for LQ_3 becomes identical to that for $\tilde{t}_1\bar{\tilde{t}}_1$ in the limit of heavy gluino, and they are very close to each other for the existing limits on gluino mass [13]. Thus, the same mass limit is applicable.

TABLE IV: 95% C.L. upper limit on the $\tilde{t}_1\bar{\tilde{t}}_1$ production cross section (in pb) as a function of $m(\tilde{t}_1)$ with our nominal choice of CTEQ6M PDFs [11] and a renormalization scale of $\sqrt{m(\tilde{t}_1)^2 + p_T^2}$. We assume $\mathscr{B}(\tilde{t}_1\bar{\tilde{t}}_1 \to \tau\tau b\bar{b}) = 1$.

		$m(\tilde{t}_1)$ (GeV$/c^2$)							
$N_{\rm evt}^{e+\tau_h}$	$N_{\rm evt}^{\mu+\tau_h}$	100	110	120	130	140	150	160	170
1	1	4.73	3.31	2.40	1.89	1.530	1.307	1.196	1.073

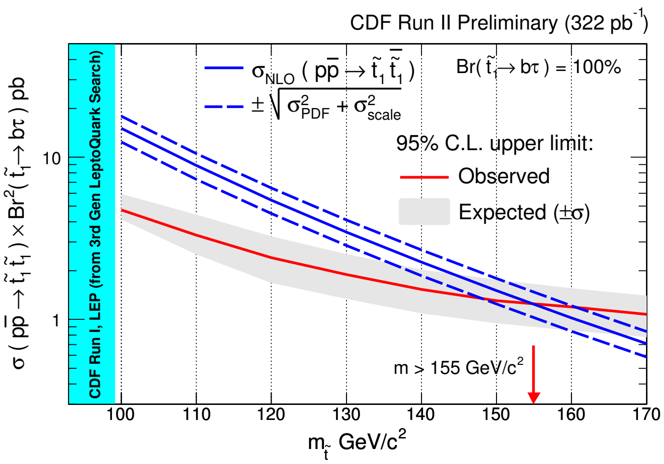

FIG. 4: 95% C.L. limit curve for the $\tilde{t}_1\bar{\tilde{t}}_1$ production cross section (thick solid line) with the NLO calculations (solid line) for the cross section [12]. The uncertainties of the theoretical calculation due to choice of PDFs and normalization scales are also shown (dashed lines). Previous constraint obtained from CDF and LEP leptoquark searches ($m(\tilde{t}_1) > 99$ GeV$/c^2$) is also shown.

VI. CONCLUSIONS

We have searched for $\tilde{t}_1\bar{\tilde{t}}_1$ production in the final state of a lepton, a τ_h and two jets using 322 pb^{-1} of $p\bar{p}$ collision data at $\sqrt{s}$ = 1.96 TeV. The final state would be expected within a $\not{R}_p$ SUSY scenario of $\tilde{t}_1 \to \tau b$. With an observation of two events that was consistent with the SM background expectation of $2.26^{+0.46}_{-0.22}$ events, we set a 95% C.L. lower limit on the $\tilde{t}_1$ mass to be 151 GeV$/c^2$ taking into account the theoretical uncertainties on the NLO cross section due to the uncertainties on Q^2 and PDFs. If no theoretical uncertainties are considered, we set the nominal 95% C.L. lower limit on the $\tilde{t}_1$ mass to be 155 GeV$/c^2$.

Acknowledgments

We thank the Fermilab staff and the technical staffs of the participating institutions for their vital contributions. This work was supported by the U.S. Department of Energy and National Science Foundation; the Italian Istituto Nazionale di Fisica Nucleare; the Ministry of Education, Culture, Sports, Science and Technology of Japan; the Natural Sciences and Engineering Research Council of Canada; the National Science Council of the Republic of China; the Swiss National Science Foundation; the A.P. Sloan Foundation; the Bundesministerium für Bildung und Forschung, Germany; the Korean Science and Engineering Foundation and the Korean Research Foundation; the Particle Physics and Astronomy Research Council and the Royal Society, UK; the Russian Foundation for Basic Research; the Comisión Interministerial de Ciencia y Tecnología, Spain; in part by the European Community's Human Potential Programme under contract HPRN-CT-2002-00292; and the Academy of Finland.

[1] H.P. Nilles, Phys. Rep. **110**, 1 (1984); H.E. Haber and G.L. Kane, *ibid*. **117**, 75 (1985). For recent review on SUSY, see S.P. Martin, "A Supersymmetry Primer," hep-ph/9709356.

[2] K. Inoue, A. Kakuo, H. Komatsu, and H. Takeshita, Prog. Theor. Phys **68**, 927 (1982); *ibid*. **71**, 413 (1984); L. Ibanez and C. Lopez, Nucl. Phys. B **233**, 511 (1984); J. Ellis and S. Rudaz, Phys. Lett. B **128**, 248 (1983).

[3] S. Weinberg, Phys. Rev. D **26**, 287 (1982); G. Farrar and S. Weinberg, *ibid*. **27**, 2732 (1983); S. Dawson, Nucl. Phys. B **261**, 297 (1985). For recent reviews on R_p violating SUSY, see H. Dreiner, hep-ph/9707435; F. de Campos *et al*., hep-ph/9903245.

[4] CDF II Collaboration, FERMILAB-PUB-96/390-E; D Acosta *et al*., Phys. Rev. D **71**, 032001 (2005).

[5] A. Anastassov *et al*., Nucl. Instrum. Methods Phys. Res. Sect. A **518**, 609 (2004).

[6] We use a coordinate system where θ and ϕ are the polar and azimuthal angles, respectively, with respect to the proton beam direction (z axis). The pseudorapidity η is defined as $-\ln[\tan(\theta/2)]$. The transverse momentum of a particle is denoted as $p_{\rm T} = p\sin\theta$. The analogous quantity using energies, defined as $E_{\rm T} = E\sin\theta$, is called transverse energy. The missing transverse energy, $\not\!\!E_{\rm T}$, is a magnitude of $\vec{\not\!\!E}_{\rm T} \equiv -\sum E^i_{\rm T}\hat{n}_i$, where $\hat{n}_i$ is the unit vector in the transverse plane pointing from the interaction point to the energy deposition in calorimeter cell i.

[7] The charged particle tracking system is enclosed in a superconducting magnet and consists of multi-layer silicon detectors and a large open-cell drift chamber (COT) covering $|\eta| < 1$. The calorimeter system is organized into electromagnetic (EM) and hadronic (HAD) sections segmented in projective tower geometry, covering $|\eta| < 3.6$. The central muon detection system is located outside of the calorimeter, used for this analysis, covering $|\eta| < 1$. The relevant detector sub-systems for this analysis are the central electromagnetic (CEM) calorimeter, central muon (CMUP) detector, and central muon extension (CMX) detector, the COT system, and the trigger system for tracks in COT (XFT).

[8] CDF Collaboration, D. Acosta *et al*., Phys. Rev. Lett. **92**, 051803 (2004).

[9] T. Sjöstrand *et al*., Comput. Phys. Commun. **135**, 238 (2001). We use PYTHIA version 6.216.

[10] R. Brun *et al*., CERN-DD/EE/81-1 (1987).

[11] CTEQ Collaboration, H.L. Lai *et al*., Eur. Phys. J. C **12**, 375 (2000).

[12] W. Beenakker, R. Höpker, M. Spira, and P. M. Zerwas, Nucl. Phys. B **492**, 51 (1997). We use PROSPINO version 2.

[13] C. Rott, FERMILAB-THESIS-2004-52.